CALPHAD: Computer Coupling of Phase Diagrams and Thermochemistry 34 (2010) 232–244

Contents lists available at ScienceDirect

CALPHAD: Computer Coupling of Phase Diagrams and Thermochemistry

journal homepage: www.elsevier.com/locate/calphad

Critical evaluations and thermodynamic optimizations of the Mn–S and the Fe–Mn–S systems

Youn-Bae Kang *

Graduate Institute of Ferrous Technology, Pohang University of Science and Technology, San 31, Hyojadong, Pohang, Kyungbuk, 790-784, Republic of Korea

ARTICLE INFO

Article history:
Received 17 December 2009
Received in revised form
21 February 2010
Accepted 19 March 2010
Available online 24 April 2010

Keywords:
Mn–S
Fe–Mn–S
Modified quasichemical model
CALPHAD
Phase diagram

ABSTRACT

Critical evaluations and thermodynamic optimizations of the manganese–sulfur binary system and iron–manganese–sulfur ternary systems have been carried out over the entire composition range from room temperature to above the liquidus temperature. The Gibbs energies of all available phases have been thermodynamically modeled, and model parameters have been optimized in order to reproduce all available and reliable experimental data simultaneously within experimental error limits. For the liquid phase, the Modified Quasichemical Model (MQM) in the pair approximation is employed in order to properly take into account short-range-ordering in the phase. Thermodynamic model parameters of binary liquid Fe–S using the MQM and those of binary liquid Fe–Mn using the random-mixing model available in the literature are combined with those of binary liquid Mn–S using the MQM from the present study, in the framework of the MQM, in order to estimate Gibbs energy of ternary liquid Fe–Mn–S. Observed ternary solid solutions: (Mn, Fe)S and $Fe_{1-x}S$ are modeled using simple random-mixing model.

1. Introduction

Liquid metal–sulfur alloy usually exhibits very strong short-range ordering (SRO) at a specific composition. For instance, an abrupt change in sulfur partial pressure of several orders of magnitude over liquid Fe–S alloy around $X_S \cong 0.5$ supports such a strong SRO in the liquid by forming Fe–S nearest-neighbor pairs [1] (similar observations have been well observed for other liquid metal–sulfur alloy such as Ni–S, Cu–S, Co–S [2]). At the similar composition where the SRO in the liquid phase is observed, also stable solid phase is usually found in phase diagrams (e.g., $Fe_{1-x}S$). Those sulfide phases, both liquid and solid, are generally important in metal processing since they appear as non-metallic inclusions, grain boundary precipitates, defects from hot shortness, etc.

Mn exhibits strong affinity to S to form MnS in steels. Traditionally, Mn has been added to steel during steelmaking process in order to prevent hot-shortness of low melting $Fe_{1-x}S$ by forming high melting (Mn, Fe)S. Recently, an attempt to utilize evenly distributed MnS inclusions in steel has been suggested [3] by which strength of the steel could be enhanced. Also, desulfurization of molten steel is closely related to interaction between Mn and S. Therefore, phase diagram and thermodynamics of the Fe–Mn–S system, in particular for Fe-rich corner, is of practical importance to steelmakers.

Thermodynamic assessments for the Fe–Mn–S systems have been carried out several times [4–7]. Due to the strong SRO in liquid phase, a simple random mixing model is not working properly to model thermodynamic properties of the liquid Fe–Mn–S phase. Most recent thermodynamic assessment by Lee et al. [7] employed the associate model for the liquid phase assuming existence of molecular-like "associate" such as "FeS", but further details were not given. Other thermodynamic assessments used two-sublattice model for the liquid phase with the following formula: (Fe, Mn)(S, Va) forming a reciprocal ternary solution, assuming random mixing of species in each sublattice [4–6]. Thus, SRO between metal (Fe and Mn) and S in the liquid phase was treated by assuming FeS and MnS molecules in the reciprocal liquid. It is seen from the above model structure that the model extends up to $X_S = 0.5$.

In the present study, the Modified Quasichemical Model (MQM) in the pair approximation [8] was used to model the liquid phase. Recently, this model has been successfully used to model Fe–S [1] and Ni–S [9] binary liquid phase, and has been extended to model Fe–Ni–S ternary liquid phase [10], from pure liquid metal to pure (hypothetical) liquid S. It has been shown by Waldner and Pelton [10] that the advantage of employing the MQM in the modeling of metal–sulfur liquid phase is two fold: one is lesser number of ternary model parameters required, compared to other models, by proper modeling SRO in the solutions, and the other is the ability of building up a multicomponent thermodynamic database where sub-systems are modeled either by the random mixing model or by the MQM. The latter is a great practical advantage for multicomponent database development. Such methodology has been proposed by Pelton and Chartrand [11], and also has been applied in

* Tel.: +82 54 279 9032; fax: +82 54 279 9299.
E-mail address: ybkang@postech.ac.kr.

0364-5916/$ – see front matter © 2010 Elsevier Ltd. All rights reserved.
doi:10.1016/j.calphad.2010.03.005

multicomponent light metal alloy database [12,13]. In the present study, Gibbs energy of Fe–Mn–S ternary liquid phase is modeled in the framework of the MQM by merging model parameters of Fe–S binary liquid modeled by Waldner and Pelton [1] using the MQM, those of Fe–Mn binary liquid modeled by Huang [14] using the random mixing model, and those of Mn–S binary liquid modeled in the present study using the MQM. For solid solutions found in the Fe–Mn–S system, simple random mixing models are used.

2. Literature review

2.1. Mn–S system

Experimental information in the Mn–S system is very limited due to high melting temperature of MnS and strong affinity of manganese to oxygen which may contaminate samples. Most feature of the Mn–S binary phase diagram was established in 1937 by Vogel and Hotop [15] who employed thermal analysis (TA) technique. They revealed that the Mn–S liquid phase exhibits a wide immiscibility between metallic liquid (L_1) and sulfidic liquid (L_2) at high temperature. They reported the melting temperature of MnS ($T_{m,\mathrm{MnS}}$), a monotectic temperature (T_{mo}, $L_2 = L_1 + \mathrm{MnS}$) and a eutectic temperature (T_{eu}, $L_1 = (\delta\mathrm{Mn}) + \mathrm{MnS}$) at 1610 ± 10 °C, 1580 °C, and 1230 °C, respectively. The melting temperature of the MnS had been in controversy among various investigations (1530 °C [16], 1620 °C [17], 1610 ± 3 °C [18], 1530 °C [19], 1620 °C [20]). Such discrepancy was attributed to oxygen contamination [15]. Later, Staffansson [21] re-investigated this system using differential thermal analysis technique under carefully controlled oxygen potential (lower than 10^{-24} atm) and obtained the melting temperature of MnS at higher temperature (1655 ± 5 °C) than the previous investigations. He also measured the monotectic temperature at 1570 ± 5 °C. Dashevsky and Kashin [22] determined liquidus composition of MnS in temperature range from 1300 to 1500 °C. This seems to be the only liquidus data in the Mn–S system. Non-stoichiometry of MnS was found to be negligible ($n_{\mathrm{S}}/n_{\mathrm{Mn}} < 1.001$) [23,24], contrary to that of FeS [1].

Coughlin measured heat contents of MnS ($H_T - H_{298\ \mathrm{K}}$) using high temperature drop calorimetry [25]. In his results, the heat contents data exhibit a jump near 1530 °C with a latent heat of 26 kJ/mol. Thus, he suggested these data as a melting temperature and heat of fusion of MnS, respectively. Heat of formation of MnS ($\Delta H_{298,\mathrm{MnS}}$) was measured by mainly calorimetry and the values were found to be in the range from −184 to − 216 kJ/mol [26–35]. After evaluation of these data, Mills proposed $\Delta H_{298,\mathrm{MnS}}$ to be −213.4 ± 2.1 kJ/mol [36]. He also proposed absolute entropy of MnS ($S_{298,\mathrm{MnS}}$) to be 80.33 ± 0.84 J/mol K after evaluation of low temperature C_p data [20,37–39].

Experimental information on S-rich region is very rare. MnS_2 seems to be stable only at low temperature and quickly dissociates into MnS(s) and $S_n(g)$ ($n = 1$ to 8) [40].

2.2. Fe–Mn–S system

An extensive review in the Fe–Mn–S system has been made recently by Tomashik and Lukas [41], therefore only some important information relevant to the present thermodynamic optimization will be discussed in detail. Stable phases in the Fe–Mn–S system are listed in Table 1. One of the most noticeable phase relations in this system is a large miscibility gap of liquid phase in Fe–Mn–MnS–FeS trapezoid. This miscibility gap starts from Mn–MnS side and ends near Fe–FeS side. Tie-lines in this immiscibility were experimentally determined by Vogel and Hotop [15] and Sano et al. [42]. Direction of the tie-lines of the miscibility gap gradually changes from Mn–MnS direction to Fe–MnS direction. This is attributed to strong attraction between Mn and S in the liquid Fe–Mn–S.

Solid FeS in hexagonal structure exhibits noticeable non-stoichiometry toward S side, and also allows dissolution of limited amount of Mn (∼0.07 in terms of $n_{\mathrm{Mn}}/(n_{\mathrm{Fe}} + n_{\mathrm{Mn}})$) [44–47]. Solid MnS in cubic structure also dissolves Fe up to 0.8 in terms of $n_{\mathrm{Fe}}/(n_{\mathrm{Fe}} + n_{\mathrm{Mn}})$ [44–47]. Shibata determined a phase diagram of "FeS"–"MnS" system ($X_{\mathrm{S}} = 0.5$) using TA, metallography and chemical analysis [18]. He reported a eutectic reaction ($L_2 = \mathrm{FeS} + \mathrm{MnS}$) at 1164 °C. However, analysis of his synthesized samples (FeS and MnS) by himself suggested that the system investigated by Shibata might not lie on a stoichiometric "FeS"–"MnS" line. Mann and Van Vlack employed an electron probe microanalysis (EPMA) to determine mutual solubilities of FeS and MnS in the "FeS"–"MnS" system where they reported their synthesized FeS sample contains slightly higher S ($X_{\mathrm{S}} \cong 0.51$) than stoichiometric FeS [44]. Also, solubilities of Fe in MnS and Mn in FeS in equilibrium with metallic phase ($(\alpha\mathrm{Fe})$, γ or $(\delta\mathrm{Fe})$) were measured by various investigators [42,44–50]. All their results are in good agreement. Vogel and Baur [51] and Vogel and Hotop [15] employed TA technique to measure various iso-plethal sections of the Fe–Mn–S system. Based on these investigations, a liquidus surface of the Fe–Mn–S system was proposed, and a ternary eutectic temperature near Fe–FeS side were reported to be at 1000 °C [15]. Dashevsky and Kashin [22] determined solubility of S in Mn-rich liquid which is in equilibrium with MnS at 1300 °C. Increasing Fe content in the liquid decreases S solubility. Iso-thermal sections at various temperatures were also measured by Kirkaldy et al. [48] at 1300 °C, and Sano et al. [42] at 1330 and 1615 °C. Vogel and Hotop [15] also measured tie-lines of samples equilibrated at 1600 °C, but the samples were not quickly quenched (cooled at 1.5 °C/s).

Due to its practical importance to ferrous metallurgy, many investigations have been carried out to measure solubility and activity of S in metallic liquid and solid metal, mainly Fe-rich side. Sherman and Chipman [52], Ban-Ya and Chipman [53], and Burylev et al. [54] equilibrated molten Fe–Mn alloy under H_2S–H_2 gas and measured equilibrium solubility of S in the molten alloy. From an equilibrium reaction ($H_2(g) + [\mathrm{S}] = 1/2H_2S(g)$) where [S] represents sulfur in molten Fe–Mn alloy, activity coefficient of the S in the molten Fe–Mn alloy could be derived. Similar technique was used by Turkdogan et al. [55] and Fischer and Schwerdtfeger [56] to measure solubility and activity of sulfur in γ phase. Fischer and Schwerdtfeger [57] also determined activity of S in cubic (Mn, Fe)S solid solution using the same technique.

3. Thermodynamic models used in the present study

The thermodynamic modelings of the Fe–S and Fe–Mn binary subsystems have been reported previously [1,14]. The binary model parameters from these studies were used directly in the present study. The thermodynamic modeling of the Mn–S binary subsystem has been carried out in the present study. The models were then used to predict the properties of the ternary phases from the optimized binary parameters, and if necessary, additional ternary parameters were introduced in order to reproduce the available ternary data.

All calculations and optimizations in the present study were performed with the FactSage thermochemical software [58,59]. The Gibbs energies of all phases of pure Fe, Mn and S were taken from Dinsdale [60]. A list of all binary phases in the three binary systems considered in the present study is given in Table 1. The following is a brief outline of the models used for these phases:

3.1. Liquid solution

Liquid metal–sulfur alloy exhibits a high degree of short-range ordering (SRO) resulting from the fact that metal–sulfur nearest-neighbor (NN) pairs are usually predominant over metal–metal

Table 1
Stable phases found in the Fe–Mn–S system.

Phase name	Pearson symbol	Space group	Prototype	Thermodynamic model	Note
Liquid[a]	–	–	–	MQM	Immiscibility
(αFe), (αMn)	*cI*2	$Im\bar{3}m$	W	Random mixing[b]	Bcc
γ	*cF*4	$Fm\bar{3}m$	Cu	Random mixing	Fcc
(δFe), (δMn)	*cI*2	$Im\bar{3}m$	W	Random mixing	Bcc
(αMn)	*cI*58	$I\bar{4}3m$	αMn	Random mixing	
(βMn)	*cP*20	$P4_132$	βMn	Random mixing	
(αS)	*oF*128	*Fddd*	αS	Stoichiometric	
(βS)	*mP*64	$P2_1/c$	βS	Stoichiometric	
(Mn, Fe)S	*cF*8	$Fm\bar{3}m$	NaCl	Random mixing	
MnS_2	*cP*12	$Pa\bar{3}$	FeS_2	Stoichiometric	
(Fe, Mn)S	*hP*4	$P6_3/mmc$	NiAs	Random mixing	
FeS	*hP*24	$P\bar{6}2c$	FeS	Stoichiometric	
$Fe_{11}S_{12}$	–	–	–	Stoichiometric	
$Fe_{10}S_{11}$	–	–	–	Stoichiometric	
Fe_9S_{10}	–	–	–	Stoichiometric	
Fe_7S_8	*hP*45	$P3_121$	Fe_7S_8	Stoichiometric	
FeS_2	*cP*12	$Pa\bar{3}$	FeS_2	Stoichiometric	

[a] Denoted as L_1, L_2 and L_3 in the text.
[b] Identical to the Compound Energy Formalism (CEF) with mixing in one sublattice [43].

and sulfur–sulfur nearest-neighbor pairs. It is known that characteristic of the metal–sulfur pair is ionic, hence composition of the SRO usually corresponds to composition of neutral metal–sulfide. For example, liquid Fe–S binary alloy exhibits a strong SRO near $X_S \cong 0.5$, while that of liquid Cu–S binary alloy shows a strong SRO near $X_S \cong 1/3$. Both SRO compositions were supported by experimental observations of sulfur potential [61]. On the other hands, to the best knowledge of the present author, there has been no experimental observation to determine SRO composition of liquid Mn–S binary alloy or experimental sulfur potential. Nevertheless, from the fact that a very stable solid compound, MnS, in the Mn–S system exists at its melting point, and similarity to other divalent metal–sulfur systems (Fe–S, Ni–S [1,9]), it is likely that the liquid Mn–S binary alloy also exhibits the SRO near $X_S \cong 0.5$.

Such a strong SRO is usually not easily described by a simple polynomial representation for excess Gibbs energy with assumption of random mixing between metal and sulfur. Therefore, various thermodynamic models have been tried to describe the SRO in the liquid metal–sulfur alloys. The associate model which assumes existence of molecular like associate has been extensively used by Chang and co-workers to model liquid metal–sulfur alloys [62–64]. This model results in good agreement with experimental data in binary systems, however, it usually requires several empirical ternary and quaternary parameters to reproduce the properties of multicomponent solutions. Drawbacks of the associate model in prediction of thermodynamic properties in ternary solution have been discussed by the present author [65,66]. Two-sublattice model has been used by a number of researchers [4–6,21,67] to describe metal–metal sulfide liquid. Guillermet et al. [68] used the same two-sublattice model but described whole metal–sulfur binary liquid by introducing vacancies on both sublattices. However, this approach has not been extended in higher order system. Kongoli et al. [2], Kongoli and Pelton [69] have used the Modified Quasichemical Model in the pair approximation [70] and they successfully applied the model in multicomponent liquid metal–sulfur alloys. Later, a complete thermodynamic modeling of Fe–S binary system including solid–liquid phase equilibria has been carried out by Waldner and Pelton [1] using the extended Modified Quasichemical Model in the pair approximation [8]. This model has been successfully extended into ternary Fe–Ni–S liquid phase [10]. In order to keep consistency with the work of Waldner and Pelton [1] for the Fe–S alloy, to build up a multicomponent database, and to properly take into account the strong SRO in the liquid metal–sulfur alloy, the same thermodynamic model [8] was used to model the liquid Mn–S and Fe–Mn–S alloy in the present study. This model has been successfully applied in other molten metal–sulfur system [1,10] as well as other liquid phases such as metallic alloy [12,13,66,71], oxide [72–75], salt [76,77], and oxysulfide [78].

All details of the model and notation have been described previously [8,71] and only a brief summary will be given here. Let us consider the binary Mn–S liquid solution. In the MQM in the pair approximation, the following pair exchange reaction between Mn and S on neighboring lattice sites is considered:

$$(\text{Mn–Mn}) + (\text{S–S}) = 2(\text{Mn–S});\ \Delta g_{\text{MnS}} \tag{1}$$

where (Mn–S) represents a first-nearest-neighbor (FNN) pair. The non-configurational Gibbs energy change for the formation of two moles of (Mn–S) pairs is Δg_{MnS}. The Gibbs energy of the solution is given by [8]:

$$G = (n_{\text{Mn}} g^{\circ}_{\text{Mn}} + n_{\text{S}} g^{\circ}_{\text{S}}) - T\Delta S^{\text{config}} + \left(\frac{n_{\text{MnS}}}{2}\right)\Delta g_{\text{MnS}} \tag{2}$$

where g°_{Mn} and g°_{S} are the molar Gibbs energies of the pure liquid Mn and S, ΔS^{config} is the configurational entropy of mixing given by randomly distributing the (Mn–Mn), (S–S) and (Mn–S) pairs in the one-dimensional Ising approximation [8,65], and n_{Mn}, n_{S} and n_{MnS} are the numbers of moles of Mn and S atoms, and those of (Mn–S) pairs, respectively.

Δg_{MnS} is the model parameter, and may be expanded in terms of the pair fractions [8]:

$$\Delta g_{\text{MnS}} = \Delta g^{\circ}_{\text{MnS}} + \sum_{i\geq 1} g^{i0}_{\text{MnS}} X^{i}_{\text{MnMn}} + \sum_{j\geq 1} g^{0j}_{\text{MnS}} X^{j}_{\text{SS}} \tag{3}$$

where $\Delta g^{\circ}_{\text{MnS}}$, g^{i0}_{MnS}, and g^{0j}_{MnS} are the parameters of the model which can be function of temperature.

The composition of maximum SRO is determined by the ratio of the coordination numbers, Z_S/Z_{Mn}, as given by the following equations [8]:

$$\frac{1}{Z_{\text{Mn}}} = \frac{1}{Z^{\text{Mn}}_{\text{MnMn}}}\left(\frac{2n_{\text{MnMn}}}{2n_{\text{MnMn}} + n_{\text{MnS}}}\right) + \frac{1}{Z^{\text{Mn}}_{\text{MnS}}}\left(\frac{n_{\text{MnS}}}{2n_{\text{MnMn}} + n_{\text{MnS}}}\right) \tag{4}$$

$$\frac{1}{Z_{\text{S}}} = \frac{1}{Z^{\text{S}}_{\text{SS}}}\left(\frac{2n_{\text{SS}}}{2n_{\text{SS}} + n_{\text{MnS}}}\right) + \frac{1}{Z^{\text{S}}_{\text{MnS}}}\left(\frac{n_{\text{MnS}}}{2n_{\text{SS}} + n_{\text{MnS}}}\right) \tag{5}$$

where $Z^{\text{Mn}}_{\text{MnMn}}$ and $Z^{\text{Mn}}_{\text{MnS}}$ are the values of Z_{Mn} respectively when all nearest neighbors of an Mn are Mn's, and when all nearest neighbors of an Mn are S's, and where Z^{S}_{SS} and $Z^{\text{S}}_{\text{MnS}}$ are defined similarly. (Note that $Z^{\text{S}}_{\text{MnS}}$ and $Z^{\text{S}}_{\text{SMn}}$ represent the same quantity and can be used interchangeably.) In order to set the composition of

Table 2
Model parameters of thermodynamic models optimized in the present study.

Liquid (L_1 or L_2 or L_3)	MQM[a] (Fe, Mn, S)
$Z_{FeFe} = Z_{FeMn} = Z_{MnFe} = Z_{MnMn} = Z_{SS} = 6$, $Z_{FeS} = Z_{SFe} = Z_{MnS} = Z_{SMn} = 2$	
Δg°_{MnS}	$-236\,396 + 16.744T$
g^{10}_{MnS}	$78\,322 - 12.552T$
g^{20}_{MnS}	16 736
g^{02}_{MnS}	31 380
Δg_{FeS}	From [1]
Δg_{FeMn}	From [14] ($=L_{Fe,Mn}$)
g^{001}_{FeS}(Mn)	10 460
(Mn, Fe)S	CEF[b] (Mn, Fe)[S]
G_{MnS}	$G^{\circ}(MnS) = -227\,939.7765 + 241.3719T - 47.6976T\ln T - 0.0037656T^2$ ($T < 1928$) [36]
G_{FeS}	G°(FeS, hp) + 3138 − 0.75312T, (G°(FeS, hp) from [1])
$L_{Mn,Fe:S}$	$7531.2 - 0.4184T$
$Fe_{1-x}S$	CEF (Fe, Va, Mn) [S]
G_{MnS}	$G^{\circ}(MnS) + 15\,899.2 + 2.092T$
	Other parameters are taken from [1]
γ	CEF (Fe, Mn, S)
$L_{Mn,S}$	0
$L_{Fe,Mn}$	From [14]
$L_{Fe,S}$	From [1]
(αFe), (δFe), (δMn)	CEF (Fe, Mn, S)
$L_{Mn,S}$	0
$L_{Fe,Mn}$	From [14]
$L_{Fe,S}$	From [1]
MnS_2	Stoichiometric compound
$G^{\circ}(MnS_2)$	$G^{\circ}(MnS_2) = -251\,057.4743 + 374.6620T - 69.70544T\ln T - 0.00883T^2 + 217\,923.64T^{-1}$

[a] The Modified Quasichemical Model.
[b] The Compound Energy Formalism.

maximum SRO at $X_S = 1/2$, (corresponding to the composition MnS) in the Mn–S system, we set the ratio $Z^S_{MnS}/Z^{Mn}_{MnS} = 1/1$. Although the model is sensitive to the ratio of the coordination numbers, it is less sensitive to their absolute values. The use of the one-dimensional Ising model in Eq. (2) introduces a mathematical approximation into the model which we have found, by experience, can be partially compensated by selecting values of Z_{Mn} and Z_S which are smaller than the actual values. The values of the coordination numbers selected in the present study are listed in Table 2.

Similarly, the binary liquid Fe–S solution was thermodynamically modeled using the MQM, and the model parameters were given previously [1].

For the binary liquid Fe–Mn alloy, degree of SRO is negligible, and a Bragg-Williams random mixing model was used with the following formula (per mole of atoms):

$$G = X_{Fe}G^{\circ}_{Fe} + X_{Mn}G^{\circ}_{Mn} + RT(X_{Fe}\ln X_{Fe} + X_{Mn}\ln X_{Mn}) + X_{Fe}X_{Mn}L_{Fe,Mn} \quad (6)$$

where X_i, G_i are mole fraction and molar Gibbs energy of component i, and $L_{i,j}$ represents an interaction energy between i and j, which can be a function of temperature and composition of Redlich–Kister type polynomial. Optimized binary parameters were taken from Huang [14].

The Gibbs energy of the ternary Fe–Mn–S liquid solution is then estimated in the framework of the MQM with the optimized binary parameters, as already mentioned in Section 1. "Toop-like" interpolation method proposed by Pelton and Chartrand [11] was used where S was assumed as an asymmetric component. Thermodynamic properties of the ternary solution estimated in this way should reproduce available experimental data as close as possible. Nevertheless, in order to obtain better agreement with the data, one small ternary adjustable parameter was introduced in the present study. Detailed mathematical expressions for the Gibbs energy of the ternary Fe–Mn–S liquid solution are given in Appendix A.

3.2. Cubic Alabandite (MnS) solid solution: (Mn, Fe)S

Solid MnS has a rock-salt type fcc structure ($cF8$, $Fm\bar{3}m$), and is stable from room temperature to its melting temperature. It dissolves up to 79 mol% FeS [41]. This phase is one of the most important phases as a non-metallic inclusion in steel. In a number of literatures, a name "Q" was assigned after a work of Vogel and Hotop [15]. However, this name has also been used for a metallic compound $Al_7Cu_3Mg_6$ [79]. Therefore, (Mn, Fe)S instead of "Q" will be used throughout this manuscript because it is easy to recognize.

A simple random mixing model with regular solution parameter was used in the present study to model this phase;

$$G = X_{MnS}G_{MnS} + X_{FeS}G_{FeS} + RT(X_{MnS}\ln X_{MnS} + X_{FeS}\ln X_{FeS}) + X_{MnS}X_{FeS}L_{MnS,FeS}. \quad (7)$$

G_{MnS} was set to equal to the molar Gibbs energy of pure solid MnS (G°_{MnS}), while G_{FeS} was varied from the molar Gibbs energy of pure stoichiometric FeS of hexagonal structure (G°_{FeS}). Therefore, ($G_{FeS} - G^{\circ}_{FeS}$) and $L_{MnS,FeS}$ were used as model parameters.

3.3. Hexagonal Pyrrhotite (FeS) solid solution: $Fe_{1-x}S$

High temperature form of solid FeS has a NiAs type hexagonal structure ($hP4$, $P6_3/mmc$) showing noticeable non-stoichiometry toward S side [1]. The non-stoichiometry is generated by Fe vacancies in octahedral sites of the hexagonal structure. It was previously modeled by Waldner and Pelton [1] using a simple random mixing model between "FeS" and "VaS", where "VaS" is a hypothetical compound where all octahedral sites are filled by "vacancy". A name "P" was assigned since a work of Vogel and Hotop [51] followed by other investigations, however, $Fe_{1-x}S$ will be used throughout the present study because it is easy to recognize. According to early investigations, MnS dissolves in the pyrrhotite solid solution up to 9 mol% [41]. And the non-stoichiometry of $Fe_{1-x}S$ is quickly reduced by the dissolution of MnS. Therefore, it is assumed in the present study that "FeS", "VaS" and "MnS" mix randomly and the following Gibbs energy expression is employed:

$$G = X_{FeS}G_{FeS} + X_{VaS}G_{VaS} + X_{MnS}G_{MnS} + RT(X_{FeS}\ln X_{FeS} + X_{VaS}\ln X_{VaS} + X_{MnS}\ln X_{MnS}) + X_{FeS}X_{VaS}L_{FeS,VaS} \quad (8)$$

where meaning of each symbol is the same as that of (Mn, Fe)S phase. G_{FeS}, G_{VaS} and $L_{FeS,VaS}$ were taken from Waldner and Pelton [1]. G_{MnS} was varied from the molar Gibbs energy of pure stoichiometric MnS of fcc structure (G°_{MnS}). Therefore, ($G_{MnS} - G^{\circ}_{MnS}$) was used as a model parameter. No interaction energy associated with MnS was introduced since solubility of MnS in the $Fe_{1-x}S$ is rather small.

3.4. Metallic solid solution: Fe(α), Fe(δ), γ, Mn(α), Mn(β), and Mn(δ)

Fe has three polymorphs, α, γ and δ while Mn has four polymorphs, α, β, γ and δ. Fe(α), Fe(δ), Mn(δ) have bcc structure ($cI2$, $Im\bar{3}m$), Fe(γ) and Mn(γ) have fcc structure ($cF4$, Fm-$3m$), while Mn(α) and Mn(β) exhibit their own structures, ($cI58$, $I\bar{4}mm$) and ($cP20$, $P4_132$), respectively. All these phases have mutual solubilities, and Fe(γ) and Mn(γ) form complete solid solution. All these phases were modeled by Huang [14] using random substitutional model. A recent thermodynamic assessment of

Witusiewicz et al. [80] results in almost same results, but more complicated parameters in the same model was used. Therefore, parameters from Huang [14] were taken in the present study without any modification. In the present study, the fcc-based solution is denoted as γ, while other solutions were denoted as Fe(α), Fe(δ), Mn(α), Mn(β), and Mn(δ). Solubility of S in Fe(α), Fe(δ), γ, and Mn(δ) were modeled using a simple random mixing model. Model parameters of Fe–S binary solutions were taken from Waldner and Pelton [1]. Contribution of magnetic properties to Gibbs energy of mixing was described by Huang [14] employing a phenomenological equation suggested by Hillert and Jarl [81], and those were taken in the present study.

3.5. Stoichiometric compounds

Properties of the stoichiometric compounds Fe_7S_8, Fe_9S_{10}, $Fe_{10}S_{11}$, $Fe_{11}S_{12}$, FeS (troilite) and FeS_2 were directly taken from Waldner and Pelton [1], while those of MnS_2 were taken from Mills [36] with slight modification in the present study. Although the FeS_2 and MnS_2 are iso-structural, nevertheless, their probable mutual solubilities were not taken into account in the present study, due to lack of experimental data.

4. Results of thermodynamic optimization

All optimized model parameters in the present study are listed in Table 2. Those of Fe–S binary system and Fe–Mn binary system can be found in relevant articles [1,14], and are not repeated here.

4.1. Mn–S system

A calculated phase diagram of complete Mn–S binary system is shown in Fig. 1. This system has two binary compounds, MnS and MnS_2. Also, a big liquid miscibility gap between Mn and MnS has been known. Most experimental information is known only for $X_S \leq 0.5$. Therefore, S-rich portion of the phase diagram shown in the Fig. 1 is only tentative. Nevertheless, it is assumed in the present study that another miscibility gap exists at $X_S \geq 0.5$, although it is metastable under 1 bar pressure due to the presence of gas phase. Metallic liquid (Mn-rich), sulfidic liquid (MnS-rich) and sulfuric liquid (S-rich) are denoted as L_1, L_2, and L_3, respectively in the present study. Thermodynamic optimization is first carried out by optimizing parameters of solid MnS first. After then, those of liquid phase were optimized by reproducing phase diagram and heat of fusion of MnS, because no experimental information is available for the single liquid phase.

Low temperature heat capacity of MnS were measured by Georges et al. [38], Huffman and Wild [39], Andrew et al. [20], and Bousquet et al. [36]. From these heat capacity data, Mills proposed $S^{\circ}_{298\ K}$ to be 80.33 ± 0.84 J/mol K [74 Mil]. In the present study, this value (80.33 J/mol K) was chosen. His proposed $H^{\circ}_{298\ K}$ (−213.4 kJ/mol) was also adopted in the present study. Heat capacity of solid MnS above room temperature may be derived from the heat contents data of Coughlin [25]. Fig. 2 shows the measured heat content data by Coughlin [25]. Except for two heat content data at high temperature showing a jump, those data were used by Mills to estimate heat capacity of solid MnS. This was also taken in the present study. Thick lines are calculated in the present study using the heat capacity function proposed by Mills [36]. Below 1500 °C, the agreement between Coughlin's data and the calculation in the present study is very good. Long dashed line is calculated heat content using parameters taken from Miettinen and Hallstedt [5], and short dashed line is calculated heat content using parameters taken from Staffansson [21], subsequently adopted by Hillert and Staffansson [4] and Ohtani et al. [6]. The latter three studies adopted an expression of Gibbs

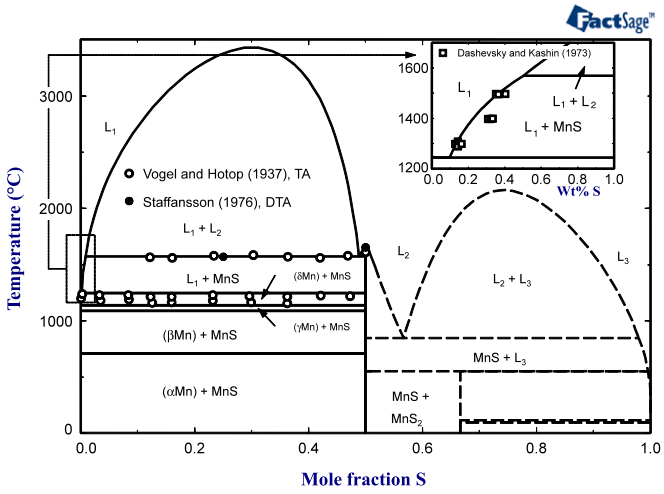

Fig. 1. Calculated phase diagram of the Mn–S system along with experimental data [15,21]. Phase diagram where $X_S > 0.5$ is only tentative and is shown as dashed line. Inset shows solubility of S in Mn-rich liquid in equilibrium with MnS, along with experimental data [22].

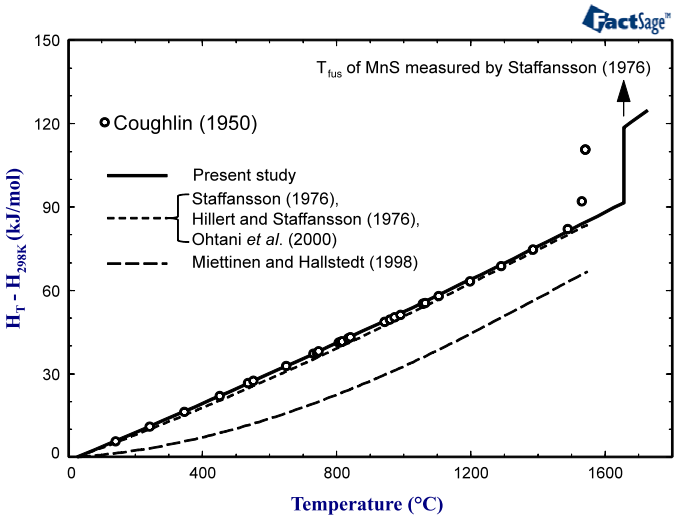

Fig. 2. Heat contents of MnS measured by drop-calorimetry along with experimental data [25]. Lines are calculated; full line from the present study, short-dashed line from Staffansson [21], Hillert and Staffansson [4], Ohtani et al. [6], long-dashed line from Miettinen and Hallstedt [5].

energy of formation of solid MnS ($Mn(\beta) + 1/2S_2(g) = MnS(s)$) by Larson and Elliott [33]. The heat contents calculated in the present study as well as Staffansson [21], Hillert and Staffansson [4] and Ohtani et al. [6] are in good agreement with the experimental data. The calculated heat content from Miettinen and Hallstedt [5] deviates from the experimental data significantly.

In his calorimetric measurement, Coughlin observed a jump in the heat content near 1530 °C as large as 26.1 kJ/mol [25]. He attributed it to melting of MnS, hence melting temperature and enthalpy of fusion were reported, respectively. This melting temperature is significantly lower than Staffansson's data (1655 ± 5 °C) who used W crucible preliminary reduced by H_2 gas and measured the melting temperature under extremely low oxygen potential ($p(O_2) < 10^{-24}$ atm). Coughlin used Pt–Rh capsule which might dissolve Mn at high temperature. Therefore, in the present study, the enthalpy of fusion of MnS was taken from Coughlin's work, but melting temperature was adopted from Staffansson's work. Resultant heat content including melting reaction is shown as thick line in Fig. 2.

Model parameters of liquid phase were mainly optimized in order to reproduce (1) melting temperature of MnS [21] ($T_{m,\mathrm{MnS}}$), (2) monotectic temperature ($L_2 = L_1 + \mathrm{MnS}$) [15,21] (T_{mo}), (3) eutectic temperature ($L_1 = \mathrm{Mn}(\delta)+\mathrm{MnS}$) [15] ($T_{\mathrm{eu}}$), (4) S solubility in Mn-rich liquid (L_1) [22], and (5) enthalpy of fusion ($\Delta H_{m,\mathrm{MnS}}$) [25]. Calculated melting temperature of MnS, the monotectic temperature, and the eutectic temperature are 1655, 1569, and 1243 °C, respectively. These are in good agreement with Staffansson's results ($T_{m,\mathrm{MnS}} = 1655 \pm 5$ °C and $T_{\mathrm{mo}} = 1570 \pm 5$ °C), and only 11 to 13 °C higher than Vogel and Hotop's results ($T_{\mathrm{mo}} = 1580$ °C and $T_{\mathrm{eu}} = 1230$ °C). However, samples in Vogel and Hotop's investigation might be contaminated by oxygen. On the other hand, Gibbs energy of fusion of MnS derived by Staffansson [21] and subsequently adopted by Hillert and Staffansson [4] and Miettinen and Hallstedt [5] gives melting temperature of MnS at 1697 °C, which is 42 °C higher than experimental observation [4]. This was attributed to the neglecting "atomic disorder" of MnS in their model [4,21]. Using the same modeling approach, however, Ohtani et al. [6] attempted to reproduce both temperatures ($T_{m,\mathrm{MnS}}$ and T_{mo}) by sacrificing the heat of fusion of MnS [25]. As shown in Fig. 2, the present model accounts for the $T_{m,\mathrm{MnS}}$, T_{mo} and the $\Delta H_{m,\mathrm{MnS}}$ simultaneously well.

Solubility of sulfur in Mn-rich liquid (L_1) was measured by Dashevsky and Kashin [22], and compared with the present calculation as shown in Fig. 1. Agreement is good around 1300 °C and 1500 °C while experimental solubility data around 1400 °C shows higher S content than the calculation as much as ~0.1 wt% S. If these data were to be reproduced, then the liquidus of MnS would have been S-shaped, which is unlikely.

According to Biltz and Wiechmann [40], MnS_2 dissociates into MnS and sulfur gas, and vapor pressure of S over MnS_2 is very close to that of pure S. In order to account for it approximately, $H^{\circ}_{298\ \mathrm{K}}$ of MnS_2 was varied from −223 844 J/mol [36] to −228 028 J/mol, and a model parameter of liquid phase in S-rich region was introduced. All other properties of MnS_2 ($S^{\circ}_{298\ \mathrm{K}}$ and C_p) were taken from Mills [36]. Introducing the model parameter of S-rich liquid results in a miscibility gap between MnS and S. This miscibility gap has not been experimentally observed yet, however, similar miscibility gaps are found in other metal–sulfur binary systems.

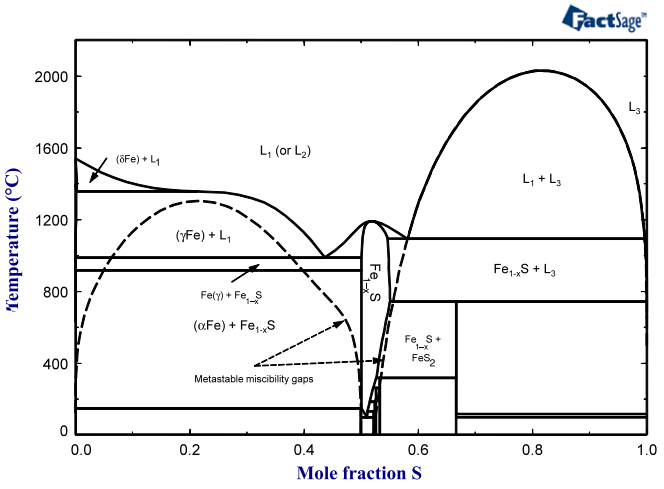

Fig. 3. Calculated phase diagram of the Fe–S system [1]. Dashed lines represent calculated metastable miscibility gaps of liquid phase.

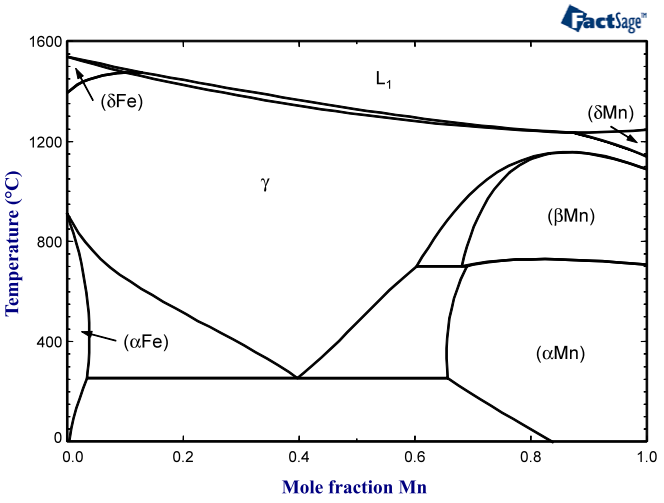

Fig. 4. Calculated phase diagram of the Fe–Mn system [14].

4.2. Fe–Mn–S system

4.2.1. FeS–MnS section and FeS–MnS saturated by metallic phases

The Gibbs energy descriptions of the Mn–S system described in the previous section was combined with those of Fe–S system optimized by Waldner and Pelton [1] and those of Fe–Mn system optimized by Huang [14]. Calculated phase diagram of the Fe–S and Fe–Mn binary systems are shown in Figs. 3 and 4, respectively.

Many experimental data are available for FeS–MnS section or FeS–MnS in equilibrium with metallic phase. Shibata measured liquidus temperature along the "FeS"–"MnS" section using thermal analysis (TA) technique [18]. Even though impurity levels in the samples and atmosphere during the experiment are concerned, this is the only experimental information as liquidus of "FeS"–"MnS" pseudo-binary system, to the best knowledge of the present author. Therefore, this data was used in the present study. He also observed single phase region of (Mn, Fe)S and two-phase region between (Mn, Fe)S and $Fe_{1-x}S$ in the "FeS"–"MnS" section using metallography [18]. However, this observation does not agree with later electron probe microanalysis (EPMA) by Mann and Van Vlack [44] and Fischer and Schwerdtfeger [56]. The latter two studies suggest higher Fe solubility in (Mn, Fe)S. This discrepancy might be attributed to incomplete solid–solid reaction in Shibata's investigation due to short annealing time (~1 h) [18], contrary to >~36 h [56] and >~40 h [44] in the other studies. Furthermore, those authors also investigated mutual solubilities of (Mn, Fe)S and $Fe_{1-x}S$ in equilibrium with metallic phase (either Fe(α) or γ), which are in good agreements with those measured by Skinner and Luce [46] and Ito et al. [45] for (Mn, Fe)S–$Fe_{1-x}S$–Fe(α) or γ equilibrium. Therefore, solid–solid phase equilibria reported by Shibata [18] were not taken into account in the present study. Mn solubilities in $Fe_{1-x}S$ were also measured [44,56]. All these data are shown in Fig. 5. Phase boundary of (Mn, Fe)S, $Fe_{1-x}S$ and liquid phase in equilibrium with metallic phases were also reported by several investigators [42,44–50], and shown in Fig. 6.

Fischer and Schwerdtfeger employed gas–solid equilibration technique to measure equilibrium sulfur potential or Mn content in (Mn, Fe)S phase in gas (H_2S–H_2 mixture)/γ/(Mn, Fe)S assembly [57]. Provided that activities of Fe and Mn in γ phase are known, for example from Huang [14], then from the experiment, activities of FeS and MnS in the (Mn, Fe)S phase can be derived. The equilibrium sulfur potential ($p(H_2S)/p(H_2)$) and Mn content in (Mn, Fe)S phase measured by Fischer and Schwerdtfeger [57] are shown in Fig. 7 as symbols. In this figure, the half-filled symbols represent the equilibrium content in (Mn, Fe)S phase in the 3-phase equilibria under fixed $p(H_2S)/p(H_2)$, while open and filled symbols represent measured sulfur potential over the (Mn, Fe)S phase of fixed composition, with and without incipient precipitation of γ phase, respectively. They also measured sulfur potential in gas (H_2S–H_2 mixture)/γ/(Mn, Fe)S/L_2 assembly. This defines equilibrium sulfur

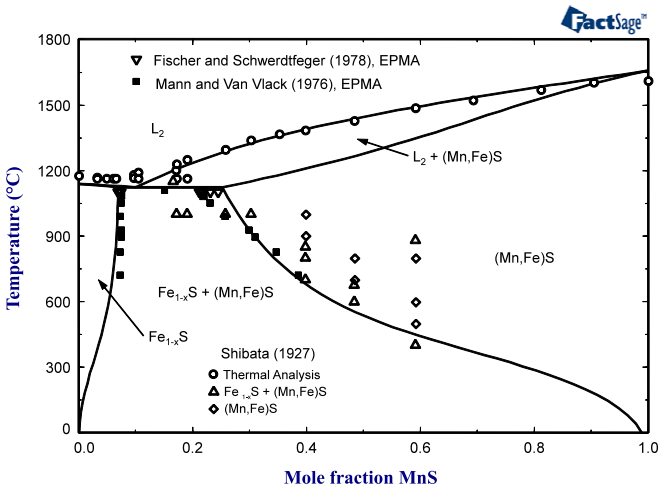

Fig. 5. Calculated phase diagram of the Fe–Mn–S system along $X_S = 0.5$ ("FeS"–"MnS" section) along with experimental data [18,44,47].

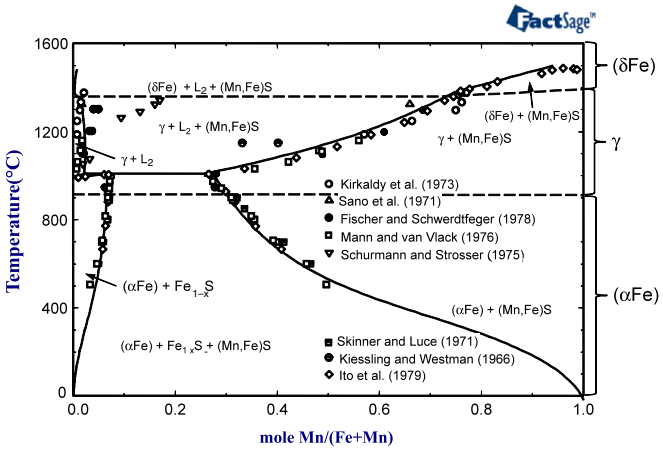

Fig. 6. Calculated equilibrium compositions of liquid (in equilibrium with γ/(Mn, Fe)S), that of (Mn, Fe)S phase (in equilibrium with γ/liquid or γ/$Fe_{1-x}S$), that of $Fe_{1-x}S$ phase (in equilibrium with γ/liquid or γ/(Mn, Fe)S), along with experimental data [42,44–50].

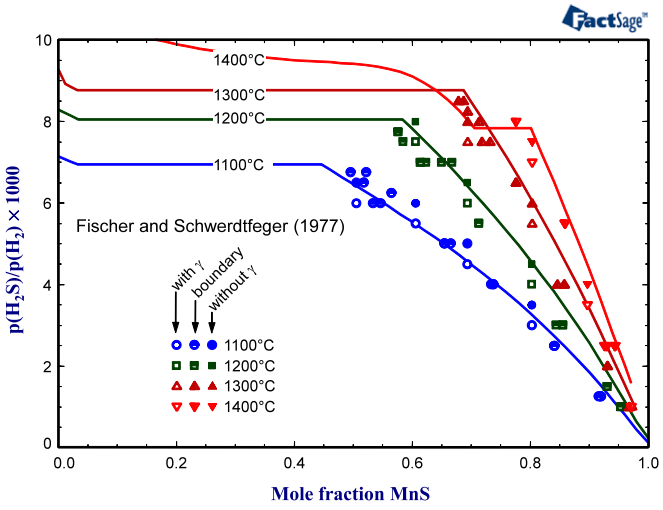

Fig. 7. Calculated $p(H_2S)/p(H_2)$ over (Mn, Fe)S phase in equilibrium with γ at various temperatures along with experimental data [57]. For the meaning of each symbol, see the text.

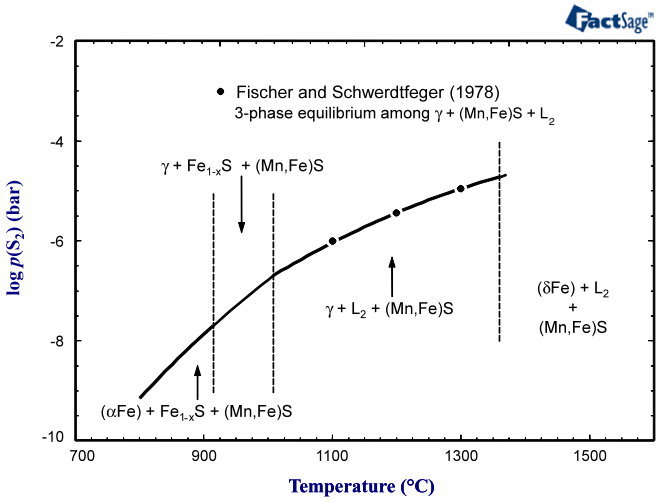

Fig. 8. Calculated equilibrium sulfur potential in various 3-phase equilibria along with experimental data for $\gamma + (Mn, Fe)S + L_2$ [47].

potential γ/(Mn, Fe)S/L_2 three-phase equilibria, which is monovariant at fixed total pressure. This is shown in Fig. 8 with solid black circles.

All these information were simultaneously used to optimize model parameters for liquid, (Mn, Fe)S and $Fe_{1-x}S$ phases. $L_{Mn,Fe:S}$ of (Mn, Fe)S phase was optimized mainly to reproduce the equilibrium sulfur potential of Fischer and Schwerdtfeger [57] in Fig. 7. Then, G_{FeS}–G°_{FeS} of (Mn, Fe)S phase and G_{MnS}–G°_{MnS} of $Fe_{1-x}S$ phase were optimized in order to reproduce solid solubility data [44–47] shown in Figs. 5 and 6. These steps were repeated until satisfactory results were obtained for solid phases. Then, the following small ternary parameter for liquid phase was added to Δg_{FeS} in order to reproduce the reported liquidus of (Mn, Fe)S phase shown in Fig. 5.

$$n_{FeS}\left[10\,460\left(\frac{X_{Mn}}{X_{Fe}+X_{Mn}}\right)\right]\ (J/mol). \tag{9}$$

Without this ternary parameter, the model calculates slightly lower liquidus of (Mn, Fe)S phase.

All lines in the Figs. 5–8 are calculated from the present thermodynamic model with the optimized parameters. Generally, good agreement was obtained. In Fig. 5, the solubility of FeS in (Mn, Fe)S along "FeS"–"MnS" section reported by Mann and Van Vlack [44] are in good agreement with the present calculation below 900 °C, but a bit higher than the present calculation above 900 °C. If the solvus of (Mn, Fe)S and $Fe_{1-x}S$ reported by those authors [44] are extrapolated to high temperature in metastable region, then they would intersect in the middle of phase diagram, which is thermodynamically improbable [82]. The solubility reported by Fischer and Schwerdtfeger [47] in the same section shows scatters. On the other hand, the agreement between experiments [44–47] and the present calculation along the section in equilibrium with metallic phase ((αFe) or γ) seems to be good as shown in Fig. 6. It seems that experimental investigation exactly on "FeS"–"MnS" was difficult compared to that in equilibrium with metallic phase. Experimentally determined solidus of (Mn, Fe)S in equilibrium with metallic phase (γ or (δFe)) [42,44,45,47,48] are in agreement with each other, also showing good agreement with the present calculation. On the other hand, "liquidus" of (Mn, Fe)S in equilibrium with γ (monovariant line of liquid phase co-saturated with γ and (Mn, Fe)S) are in conflict each other [44,47–49]. The present calculation agrees with the results showing low Mn content in the liquid [44,48]. In Fig. 7, the calculated sulfur potential in a form of $(p(H_2S)/p(H_2))$ are shown

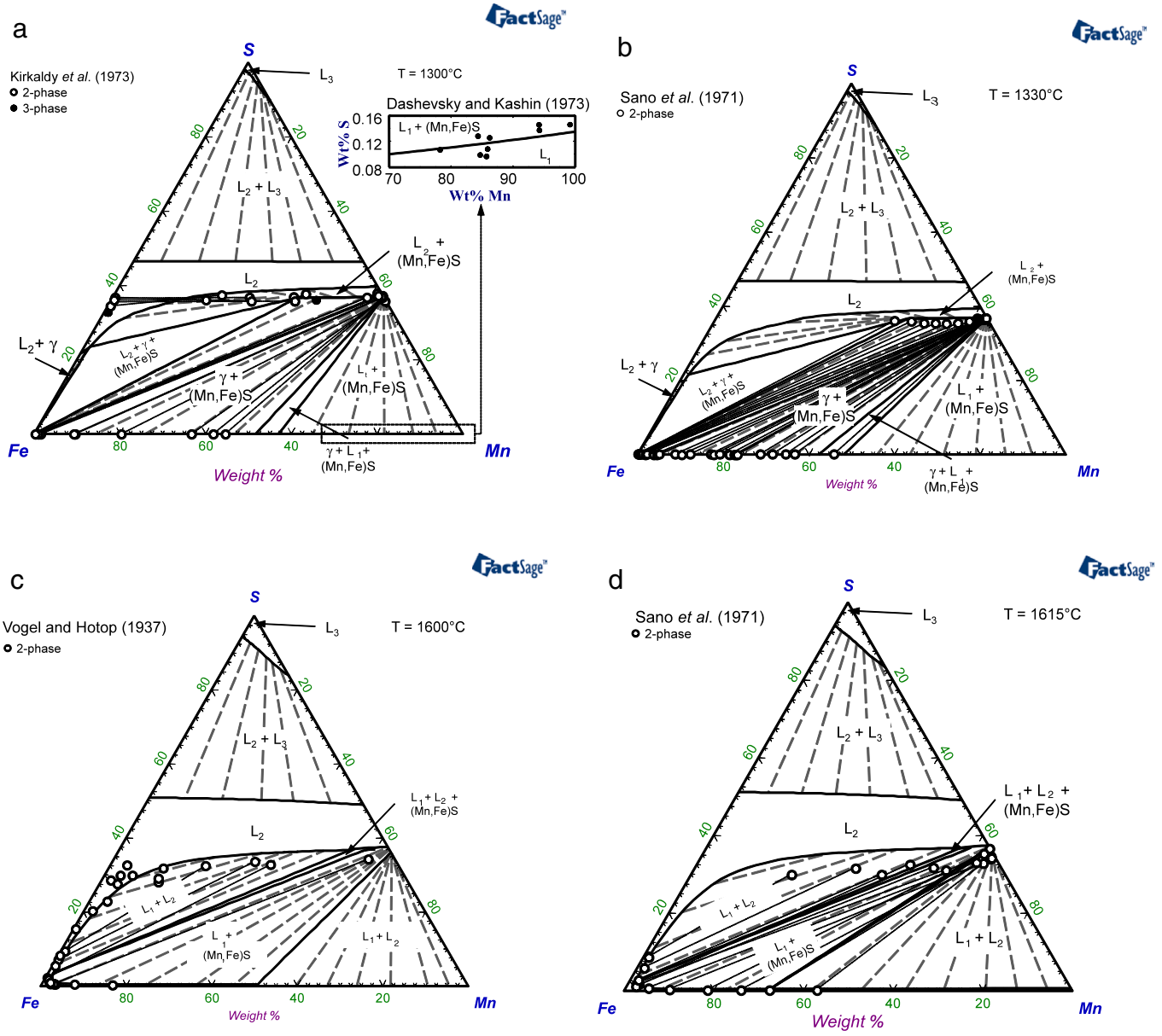

Fig. 9. Calculated isothermal sections of the Fe–Mn–S system at (a) 1300 °C, (b) 1330 °C, (c) 1600 °C, and (d) 1615 °C along with experimental data [15,22,42,48]. Dashed lines are calculated tie-lines and dotted lines are reported tie-lines. Calculated solubility of S in Mn-rich liquid alloy in equilibrium with (Mn, Fe)S is also shown as inset of (a).

along with the experimental data of Fischer and Schwerdtfeger [57]. Horizontal lines of the calculated curves are due to appearance of liquid phase. The agreement is good, and this ensures that the model parameters for (Mn, Fe)S phase are based not only on the phase equilibria but also on its thermodynamic properties. Subsequently optimized model parameter of liquid phase to reproduce liquidus of the (Mn, Fe)S phase (Fig. 5) seems also to be reasonable. Calculated equilibrium sulfur potential in gas + γ + (Mn, Fe)S + L_2 is also in good agreement with experimental data [47] as shown in Fig. 8.

4.2.2. Isothermal and isoplethal sections

A number of investigations were carried out by several authors in order to locate liquidus and other phase boundaries in the Fe–Mn–S system. Shown in Fig. 9(a)–(d) are calculated isothermal sections of the Fe–Mn–S system at 1300, 1330, 1600 and 1615 °C using the optimized model parameters along with reported experimental data [15,22,42,48]. Thick lines are calculated phase boundary and dashed lines are calculated tie-lines between 2-phase equilibria. The isothermal sections of the Fe–Mn–S system at this temperature range are predominantly characterized by wide miscibility gap (L_1 + L_2) emanating from Mn–MnS side, and liquid (L_1 or L_2) – (Mn, Fe)S phase equilibrium. Another miscibility gap when $X_S > 0.5(L_2 + L_3)$ are only tentatively drawn from the present thermodynamic model, and no experimental information is available. Therefore, it should not be read as a true stable miscibility gap unless further experimental investigation confirms it. Some experimental data were plotted in the figures with reported tie-lines (dotted-line). Experimental data of Kirkaldy et al. [48] suggested much high S content in "FeS" phase in MnS–FeS equilibrium or MnS–FeS-γ equilibrium at 1300 °C. However, such high S contents in liquid phase are not consistent with liquidus of γ phase in binary Fe–S system, nor in agreement with another experimental data of Fischer and Schwerdtfeger [47] shown in Fig. 10(c). Also, low S content in upper-end of tie-line in L_1+L_2 equilibria by Sano et al. [42] in Fig. 9(d) are also questionable.

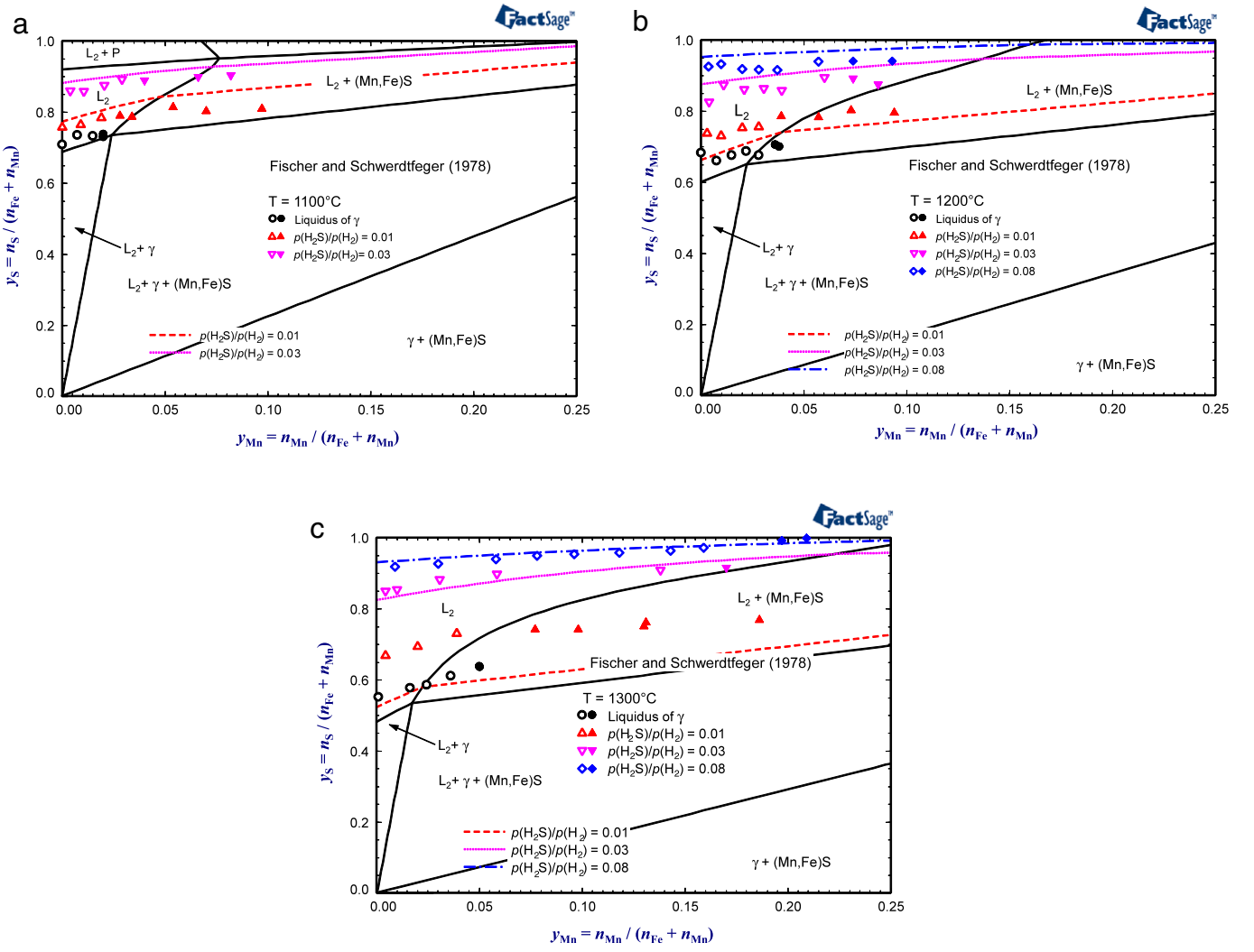

Fig. 10. Calculated isothermal sections and iso-$p(H_2S)/p(H_2)$ lines in Fe-rich corner at (a) 1100 °C, (b) 1200 °C and (c) 1300 °C. Experimental data are from Fischer and Schwerdtfeger [47] where solid symbols and open symbols stand for composition of liquid phase with (Mn, Fe)S and without (Mn, Fe)S phase, respectively.

Except for this, the present calculations reproduce the measured equilibria of γ + (Mn, Fe)S [42,48], L_1 + (Mn, Fe)S [15,22,42].

Majority of the reported tie-lines in L_1+L_2 equilibria are parallel to Fe–MnS direction, while some of them at low Mn content do not keep the direction but slightly rotated to Fe–FeS direction as seen in Fig. 9(c) and (d) [15,42]. In previous thermodynamic assessments by Hillert and Staffansson [4] and Ohtani et al. [6], they pointed out that the reported tie-lines of at the low Mn content were not accounted for by their thermodynamic analyses. On the other hand, another thermodynamic assessment by Miettinen and Hallstedt [5] nevertheless reproduced the reported tie-line [15] using adjustable ternary parameters. In the present study, after introducing the ternary parameter in the liquid phase as discussed in Section 4.2.1, tie-lines in the L_1+L_2 region are calculated. As shown in the figures, they are also not in agreement with the tie-lines [15,42] in the low Mn region, although those directing Fe–MnS side are in good agreement with the present calculation. In the present study, it was decided not to take those data into consideration during the optimization because inherent difficulties associated in this system at high temperature (oxygen contamination and quenching), thus no other adjustable parameter was attempted. Fig. 10(a)–(c) shows calculated isothermal sections at 1100 to 1300 °C in Fe-rich corner. Iso-$(p(H_2S)/p(H_2))$ lines are also calculated and shown in the figures. Experimental data of Fischer and Schwerdtfeger [47] are plotted for comparison. Solid symbols represent sample compositions in which solid (Mn, Fe)S was observed, while open symbols represent those of single liquid phase. As regard for the iso-activity curves, except for one iso-$(p(H_2S)/p(H_2))$ line of the lowest sulfur potential at 1300 °C which is also not in consistent with other investigation in Fe–S binary system [1], the present calculations are in good agreement with the experimental data. On the other hand, liquid compositions co-saturated by γ and (Mn, Fe)S show disagreement as temperature increases. It may also be noticed in Fig. 6 where the calculated liquid (L_2) composition in equilibrium with γ and (Mn, Fe)S show opposite trend to those of Fischer and Schwerdtfeger [47]. This will be discussed later.

Four isoplethal sections were measured by Vogel and Hotop [15] using TA. All these sections lie on constant Fe/Mn mass ratio directing to S corner. The present calculations reasonably reproduce most of thermal arrests, as shown in Fig. 11(a)–(d). For a reference, a calculated Fe–S phase diagram shown in Fig. 3 is also superimposed as dashed lines in Fig. 11(a) on a weight basis. Three thermal arrest points in the middle of Fig. 11(a) ($20 < \text{wt\%S} < 30$, $1050 < T\,(°C) < 1200$) do not correspond to any reactions in the present thermodynamic calculation. Those were interpreted by Vogel and Hotop [15] as thermal arrest for the reaction $L_2 \rightarrow \text{MnS} + \gamma$. Moreover, another 3 points above the former 3 points were interpreted by the authors as liquidus of MnS being a primary phase. However, from the shape of liquidus of γ in Fe–S binary system [1] and the fact that the section in Fig. 11(a)

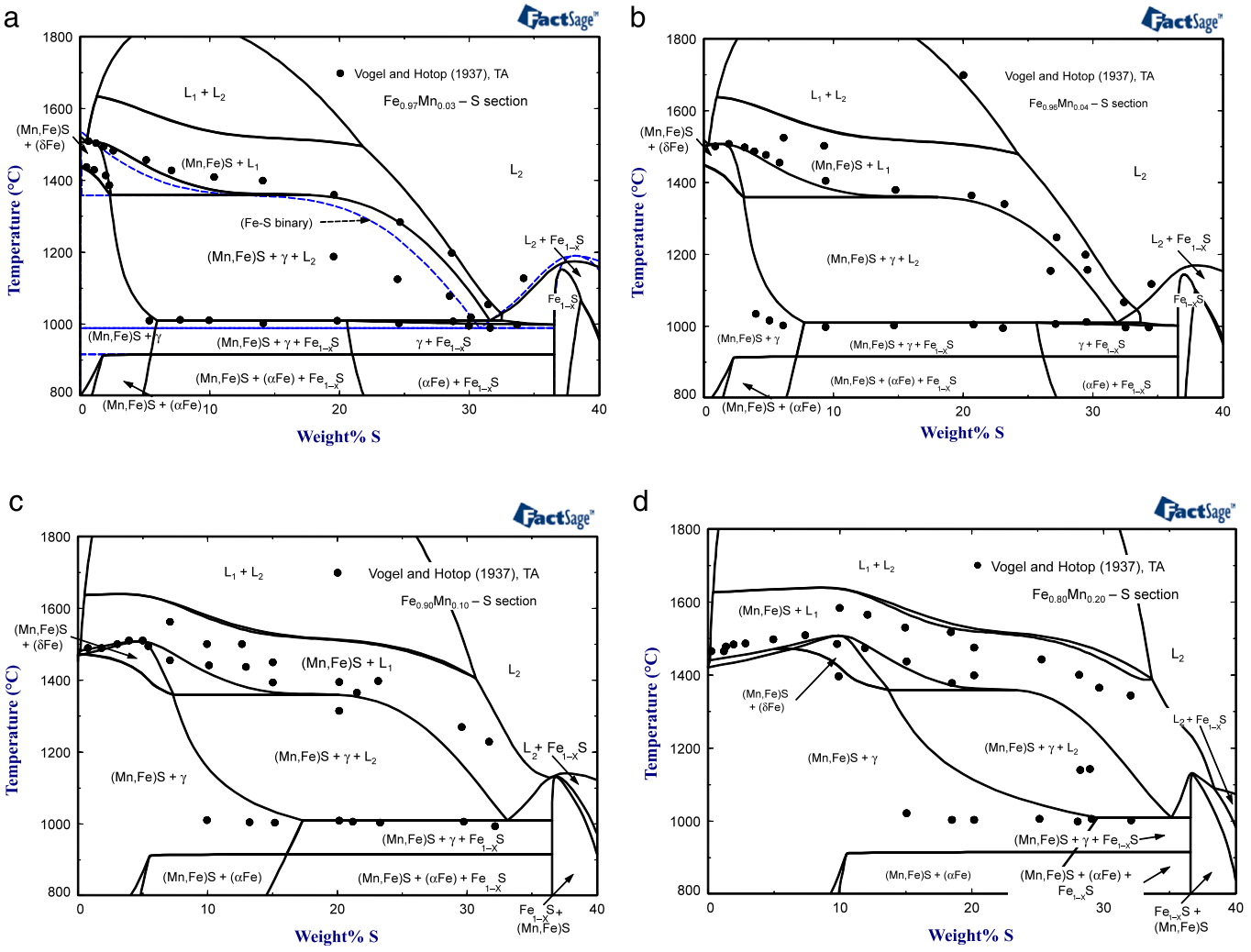

Fig. 11. Calculated isoplethal sections of Fe–Mn–S system along (a) Fe/Mn = 97/3, (b) Fe/Mn = 96/4, (c) Fe/Mn = 90/10, and (d) Fe/Mn = 80/20 (wt%), along with experimental data [15]. Dashed line in (a) is a calculated Fe–S binary phase diagram.

(and Fig. 11(b)) is very close to the binary Fe–S system, the above 3 thermal arrest are likely to be results of solidification reaction of γ phase. As shown in the figure, they are interpreted as $L_2 \rightarrow$ (Mn, Fe)S $+ \gamma$ in the present study, while no reaction could be suggested for the lower 3 points. In Fig. 11(b)–(d), thermal arrests at high temperature seem to represent $L_2 \rightarrow$ MnS $+ L_1$ reaction, which are located approximately 50 °C lower than the present calculation. However, Vogel and Hotop [15] also suggested that their samples might be contaminated by oxygen as their $T_{m,\mathrm{MnS}}$ was lower than the accepted T_m as low as 50 °C. Therefore, it may be concluded that the present calculation is acceptable.

Figs. 12 and 13 show experimentally determined solubility of S in γ phase in equilibrium with (Mn, Fe)S phase [42,55,56], and corresponding sulfur potential [55,56]. The calculations are shown as lines, and agreement is reasonable. No attempt was tried to evaluate parameters for Mn–S interaction in γ as well as any solid metallic phase ($(\alpha$Mn), $(\beta$Mn) and $(\delta$Mn)) because no experimental S solubility data in solid Mn are available, and even if the parameters are introduced, those would not significantly affect on the agreement in Figs. 12 and 13.

Fig. 14 shows a calculated liquidus projection of the Fe–Mn–S in Fe-rich corner, along with reported liquid compositions for univariant reactions [42,44,45,47–49]. Except for some data of Ito et al. [45], all other data represent compositions of liquid phase in equilibrium with γ and (Mn, Fe)S phase. Due to inherent experimental difficulty of quenching the samples, those experimental

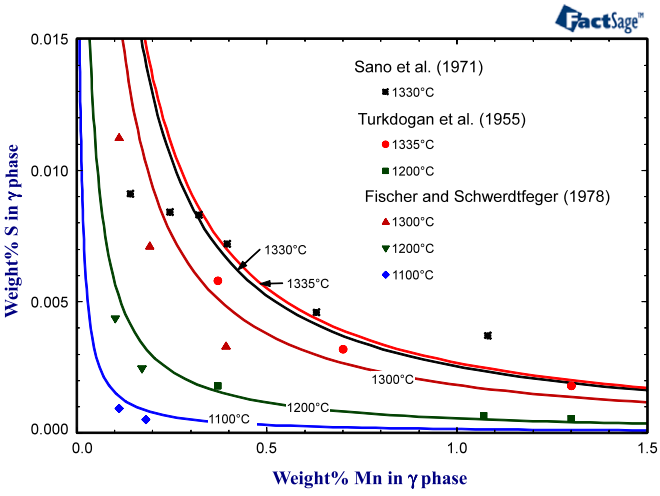

Fig. 12. Calculated solubility of S in γ in equilibrium with (Mn, Fe)S phase at various temperatures along with experimental data [42,47,55].

data do not agree each other. Schuermann and Stroesser [49] suggested too high Mn content (up to 12 wt%) of liquid phase in equilibrium with γ and (Mn, Fe)S phase. On the other hand, Kirkaldy et al. [48], Sano et al. [42] and Mann and Van Vlack [44] suggested

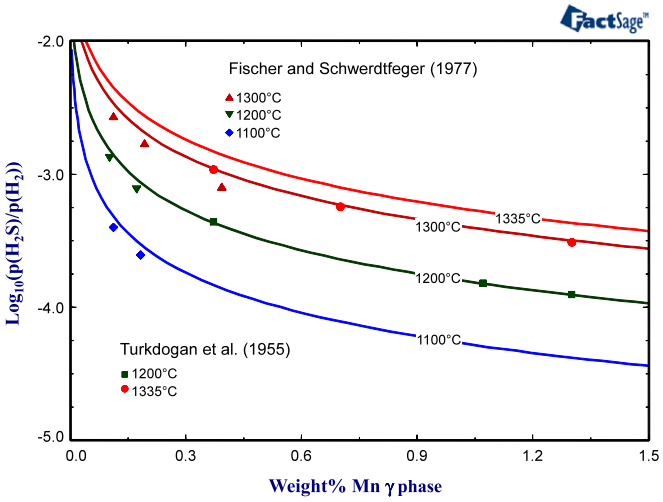

Fig. 13. Calculated activity of S expressed as $p(H_2S)/p(H_2)$ over γ in equilibrium with (Mn, Fe)S phase at various temperatures along with experimental data [47,55].

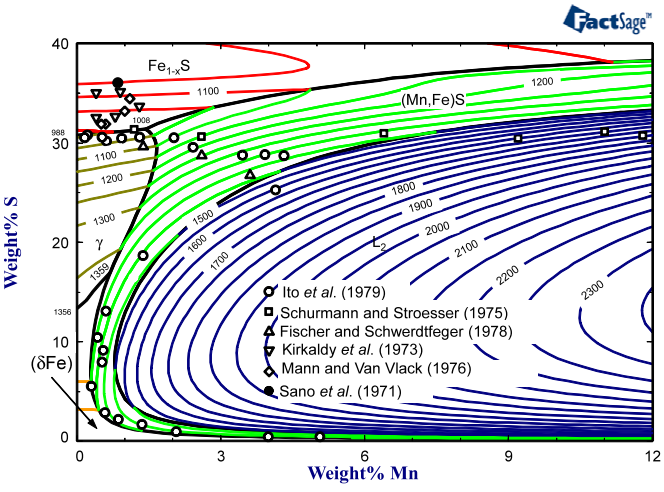

Fig. 14. Calculated liquidus surface of the Fe–Mn–S system in Fe-rich corner. Symbols are experimental data showing liquid compositions of univariant reactions [42,44,45,47–49].

lower Mn content of liquid (<∼1.3 wt%Mn) for the same equilibria. Data of Ito et al. [45] and Fischer and Schwerdtfeger [47] show that Mn content of liquid phase for the same equilibria would extend up to 4–5 wt%. It is not easy to conclude which data set is right or not. Nevertheless, the present calculation shows relatively low Mn content in liquid phase (<∼1.5 wt%Mn) for the reaction $L_2 \rightarrow \gamma +$ (Mn, Fe)S, which qualitatively agrees with the experimental data of Sano et al. [42], Kirkaldy et al. [48], and Mann and Van Vlack [44] and previous thermodynamic calculation by Hillert and Staffansson [4]. However, this monovariant line is of practical importance in ferrous metallurgy for sulfide inclusion precipitation. Therefore, it is suggested that further careful investigation be carried out.

4.2.3. Thermodynamics of liquid phase

Activity and solubility of S in Fe-rich molten Fe–Mn alloy were experimentally measured using gas (H_2S–H_2)/liquid equilibration [52–54]. The measured solubilities of S in Fe–Mn alloy under fixed sulfur potential at steel refining temperature (1550 °C to 1600 °C) are shown in Fig. 15. Also shown are calculated liquidus of (Mn, Fe)S at 1600 °C and iso-$p(S_2)$ curves. Agreement between the experiments and the calculations is very good. Under a constant S_2 potential, solubility of S increases as Mn content increases. This shows well-known attraction between Mn and S in liquid Fe.

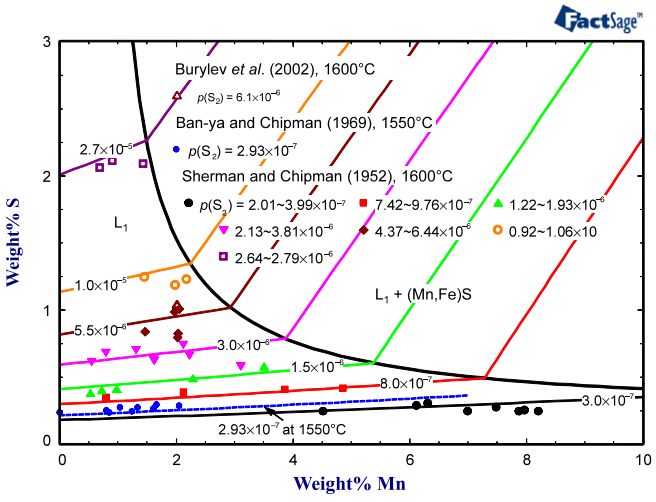

Fig. 15. Calculated solubility of S in liquid Fe–Mn alloy in equilibrium with gas phase of various $p(S_2)$ at 1550 °C and 1600 °C, along with experimental data [52–54]. A thick line represents solubility limit of S.

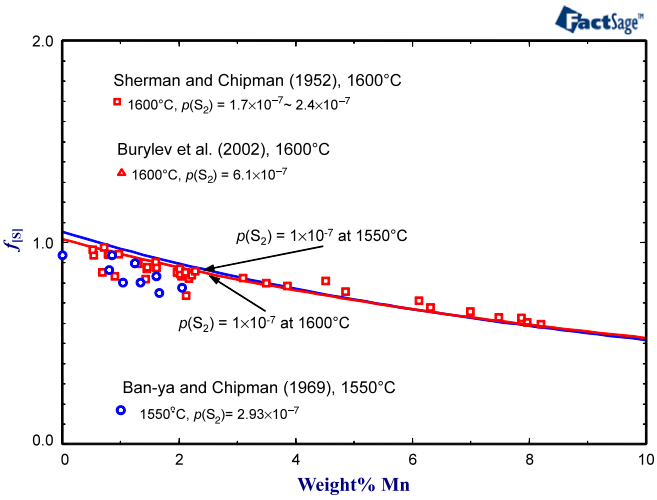

Fig. 16. Calculated activity coefficient of S ($f_{[S]}$) in the liquid Fe–Mn alloy, along with experimental data [52–54].

Therefore, activity coefficient of S should decrease as Mn content increases, and this is shown in Fig. 16. The activity coefficient of S is expressed as $f_{[S]}$ on a 1 wt% standard basis which is more practical to use.

$$\frac{1}{2}S_2(g) = [S]; \qquad \Delta G = -125\,100 + 18.5T \text{ (J)} \quad [83] \tag{10}$$

$$K = \frac{a_{[S]}}{pS_2^{1/2}} = \frac{f_{[S]}[\text{wt\%S}]}{pS_2^{1/2}} = \exp\left(\frac{-\Delta G}{RT}\right). \tag{11}$$

Although experiments were conducted under various sulfur potentials as shown in Fig. 15, the calculations in Fig. 16 were performed at $p(S_2) = 1 \times 10^{-7}$, which ensures wide single liquid region. From the calculation at 1600 °C, an interaction parameter for Wagner Formalism e_S^{Mn} may be derived, and the derived value is −0.0267, which is in good agreement with a compiled value −0.026 [84]. It should be noted that the e_S^{Mn} value which is a thermodynamic quantity of dilute region is well predicted even without any ternary model parameter of the liquid phase ($e_S^{Mn} =$ −0.028 without ternary parameter).

5. Conclusions

Critical evaluations and optimizations of the Mn–S and Fe–Mn–S systems have been presented. All available thermodynamic and phase equilibrium data have been critically evaluated to obtain one set of optimized model parameters of the Gibbs energies of all phases that can reproduce the experimental data within experimental error limits. In order to take into account a large degree of short-range ordering (SRO) in the Mn–S binary liquid phase, the Modified Quasichemical Model (MQM) in the pair approximation has been used [8]. In the framework of the MQM for multicomponent solution developed by Pelton and Chartrand [11], the optimized model parameters of the MQM for the liquid Mn–S have been merged with already optimized model parameters of the MQM for the liquid Fe–S [1], and those of the random mixing model for the liquid Fe–Mn [14]. Solid solutions in the ternary Fe–Mn–S system have been thermodynamically modeled using simple random mixing models. The present thermodynamic optimization can be used as a part of a multicomponent thermodynamic database for metal–sulfur systems.

Appendix A. Gibbs energy of ternary liquid Fe–Mn–S solution in the framework of the Modified Quasichemical Model in the pair approximation

As described in Section 3.1, the Gibbs energy of ternary Fe–Mn–S liquid solution was described in the framework of the Modified Quasichemical Model (MQM) in the pair approximation [8,11]. Among three sub-binary solutions, two of them (Fe–S and Mn–S) were described using the MQM in the pair approximation while the other (Fe–Mn) was described using random mixing model. In Appendix A, how those 3 binary modeling can be merged into one general solution model. It was originally demonstrated by Pelton and Chartrand [11] for general case in multicomponent solution, but the general expression is now reduced to the Fe–Mn–S ternary solution case in Appendix A.

The Gibbs energy of the ternary solution is written in the framework of the MQM [11]:

$$G = \left(n_{\mathrm{Fe}}g^{\circ}_{\mathrm{Fe}} + n_{\mathrm{Mn}}g^{\circ}_{\mathrm{Mn}} + n_{\mathrm{S}}g^{\circ}_{\mathrm{S}}\right) - T\Delta S^{\mathrm{config}} + \left(\frac{n_{\mathrm{FeS}}}{2}\right)\Delta g_{\mathrm{FeS}} + \left(\frac{n_{\mathrm{MnS}}}{2}\right)\Delta g_{\mathrm{MnS}} + \left(\frac{n_{\mathrm{FeMn}}}{2}\right)\Delta g_{\mathrm{FeMn}} \quad (A.1)$$

where $\Delta S^{\mathrm{config}}$ is given as [11]:

$$\Delta S^{\mathrm{config}} = -R\left(X_{\mathrm{Fe}}\ln X_{\mathrm{Fe}} + X_{\mathrm{Mn}}\ln X_{\mathrm{Mn}} + X_{\mathrm{S}}\ln X_{\mathrm{S}}\right) - R\left[n_{\mathrm{FeFe}}\ln\left(\frac{X_{\mathrm{FeFe}}}{Y^2_{\mathrm{Fe}}}\right) + n_{\mathrm{MnMn}}\ln\left(\frac{X_{\mathrm{MnMn}}}{Y^2_{\mathrm{Mn}}}\right) + n_{\mathrm{SS}}\ln\left(\frac{X_{\mathrm{SS}}}{Y^2_{\mathrm{S}}}\right) + n_{\mathrm{FeS}}\ln\left(\frac{X_{\mathrm{FeS}}}{2Y_{\mathrm{Fe}}Y_{\mathrm{S}}}\right) + n_{\mathrm{MnS}}\ln\left(\frac{X_{\mathrm{MnS}}}{2Y_{\mathrm{Mn}}Y_{\mathrm{S}}}\right) + n_{\mathrm{FeMn}}\ln\left(\frac{X_{\mathrm{FeMn}}}{2Y_{\mathrm{Fe}}Y_{\mathrm{Mn}}}\right)\right] \quad (A.2)$$

where Y_i is an equivalent fraction of a species i.

The above equations are identical to the model equations of the MQM for a ternary solution when all sub-binary solutions are modeled using the MQM in the pair approximation.

Since the binary Fe–Mn solution was modeled using the random mixing model, the followed equation may be suggested [11].

$$n_{\mathrm{FeMn}} = \left[Z^{\mathrm{Fe}}_{\mathrm{FeFe}}n_{\mathrm{Fe}} + Z^{\mathrm{Mn}}_{\mathrm{MnMn}}n_{\mathrm{Mn}} + Z^{\mathrm{S}}_{\mathrm{SS}}n_{\mathrm{S}}\right]Y_{\mathrm{Fe}}Y_{\mathrm{Mn}}\ [11]. \quad (A.3)$$

This represents that total number of (Fe–Mn) pairs are assumed to be a product between total number of all kinds of pairs in a random mixing solution and probability to find the (Fe–Mn) pair in the random mixture.

Furthermore, the binary model parameters Δg_{FeS}, Δg_{MnS} and Δg_{FeMn} are written in the following formula in the ternary Fe–Mn–S solution [11]:

$$\Delta g_{\mathrm{FeS}} = \Delta g^{\circ}_{\mathrm{FeS}} + \sum_{i\geq 1}(X_{\mathrm{FeFe}} + X_{\mathrm{FeMn}} + X_{\mathrm{FeMn}})^i g^{i0}_{\mathrm{FeS}} + \sum_{j\geq 1}(X_{\mathrm{SS}})^j g^{0j}_{\mathrm{FeS}} + \sum_{\substack{i\geq 0\\ j\geq 0\\ k\geq 1}}(X_{\mathrm{FeFe}} + X_{\mathrm{FeMn}} + X_{\mathrm{FeMn}})^i \times (X_{\mathrm{SS}})^j\left(\frac{X_{\mathrm{Mn}}}{X_{\mathrm{Fe}} + X_{\mathrm{Mn}}}\right)^k g^{ijk}_{\mathrm{FeS(Mn)}} \quad (A.4)$$

$$\Delta g_{\mathrm{MnS}} = \Delta g^{\circ}_{\mathrm{MnS}} + \sum_{i\geq 1}(X_{\mathrm{FeFe}} + X_{\mathrm{FeMn}} + X_{\mathrm{FeMn}})^i g^{i0}_{\mathrm{MnS}} + \sum_{j\geq 1}(X_{\mathrm{SS}})^j g^{0j}_{\mathrm{MnS}} \quad (A.5)$$

$$\Delta g_{\mathrm{FeMn}} = \sum_{i\geq 1} L^i_{\mathrm{FeMn}}\left(\frac{Y_{\mathrm{Fe}} - Y_{\mathrm{Mn}}}{Y_{\mathrm{Fe}} + Y_{\mathrm{Mn}}}\right)^i. \quad (A.6)$$

Since one ternary parameter introduced in the present study represents an effect of Mn upon (Fe–S) pair energy, the last term in Eq. (A.4) is written. No other term was required in the present study.

The Eqs. (A.2)–(A.6) are now substituted to Eq. (A.1) in order to give a complete mathematical equation of the ternary Fe–Mn–S liquid solution. It can be easily seen that if there is no Mn (or Fe), then the model equation is reduced to the MQM model equation for the binary Fe–S (or Mn–S) liquid solution. If there is no S, then the model equation is reduced to the random mixing model equation for the binary Fe–Mn liquid solution along with ideal configurational entropy of mixing in Eq. (A.2). Therefore, it has shown that how those 3 binary modeling can be merged into one general solution model.

Appendix B. Supplementary data

Supplementary data associated with this article can be found, in the online version, at doi:10.1016/j.calphad.2010.03.005.

References

[1] P. Waldner, A.D. Pelton, J. Phase Equilib. Diffus. 26 (2005) 23–38.
[2] F. Kongoli, A.D. Pelton, Y. Dessureault, Metall. Mater. Trans. B 29 (1998) 591–601.
[3] H. Mabuchi, R. Uemori, M. Fujioka, ISIJ Int. 36 (1996) 1406–1412.
[4] M. Hillert, L. Staffansson, Metall. Trans. B 7 (1976) 203–211.
[5] J. Miettinen, B. Hallstedt, CALPHAD 22 (1998) 257–273.
[6] H. Ohtani, K. Oikawa, K. Ishida, High Temp. Mater. Processes (London) 19 (2000) 197–210.
[7] B.-J. Lee, B. Sundman, S.-I. Kim, K.G. Chin, ISIJ Int. 47 (2007) 163–171.
[8] A.D. Pelton, S.A. Degterov, G. Eriksson, C. Robelin, Y. Dessureault, Metall. Mater. Trans. B 31 (2000) 651–659.
[9] P. Waldner, A.D. Pelton, Int. J. Mat. Res. 95 (2004) 672–681.
[10] P. Waldner, A.D. Pelton, Metall. Mater. Trans. B 35 (2004) 897–907.
[11] A.D. Pelton, P. Chartrand, Metall. Mater. Trans. A 32 (2001) 1355–1360.
[12] Y.-B. Kang, C. Aliravci, P.J. Spencer, G. Eriksson, C.D. Fuerst, P. Chartrand, A.D. Pelton, JOM 61 (2009) 75–82.
[13] I.-H. Jung, D.-H. Kang, W.-J. Park, N.-J. Kim, S.-H. Ahn, CALPHAD 31 (2007) 192–200.
[14] W. Huang, CALPHAD 13 (1989) 243–252.
[15] R. Vogel, W. Hotop, Arch. Eisenhuettenwes. 11 (1937) 41–54.
[16] E.N. Silverman, Trans. Metall. Soc. AIME 221 (1961) 512–517.
[17] G. Roehl, Stahl Eisen 33 (1913) 565–567.
[18] Z. Shibata, Tech. Rep. Tohoku Imp. Univ. 7 (1928) 279–289.
[19] O. Glasser, Centralbl. Mineral. Geol. Palaeontol. Abh. Abt. A (1926) 81–96.
[20] J.H. Andrew, W.R. Maddocks, E.A. Fowler, J. Iron Steel Inst. 124 (1931) 295–325.
[21] L. Staffansson, Metall. Trans. B 7 (1976) 131–134.
[22] V.Ya Dashevsky, V.I. Kashin, Izv. Akad. Nauk SSSR Met. 5 (1973) 85–88.
[23] H. Rau, J. Phys. Chem. Solids 39 (1978) 339–343.
[24] K. Nishida, T. Narita, T. Tani, G. Sasaki, Oxid. Met. 14 (1980) 65–83.
[25] J.P. Coughlin, J. Am. Chem. Soc. 72 (1950) 5445–5447.
[26] J. Thomsen, Thermodchemische Untersuchungen, Barth, Leipzig, 1882.

[27] D. Berthelot, Ann. Chim. Phys. 4 (1885) 476.
[28] A. Konnecker, W. Biltz, Z. Anorg. Allg. Chem. 242 (1967) 226.
[29] A.F. Kapostinskii, I.A. Korshunov, Acta Phys. Chim. 10 (1939) 259.
[30] J.H.E. Jeffs, F.D. Richardson, J. Pearson, Trans. Faraday Soc. 50 (1954) 364–370.
[31] L.H. Adami, E.G. King, U.S. Bur. Mines Rep. Invest. (1964) 6495.
[32] E.W. Dewing, F.D. Richardson, J. Iron Steel Inst. 195 (1960) 56–58.
[33] H.R. Larson, J.F. Elliott, Trans. AIME 239 (1967) 1713.
[34] T. Uno, K. Kanbara, E. Homma, Tetsu to Hagane 36 (1950) 479–485.
[35] H. Gamsjaeger, Monatsh. Chem. 98 (1967) 1803.
[36] K.C. Mills, Thermodynamic Data for Inorganic Sulphides, Selenides and Tellurides, Butterworths, London, 1974.
[37] J. Bousquet, M. Diot, M. Robin, C. R. Hebd. Seances Acad. Sci. Paris, Ser. C 267 (1968) 861.
[38] R. Georges, E. Gmelin, D. Landau, J.C. Lasjaunias, C. R. Hebd. Seances Acad. Sci. Paris, Ser. B 269 (1969) 827.
[39] D.R. Huffman, R.L. Wild, Phys. Rev. 148 (1966) 526–527.
[40] W. Biltz, F. Wiechmann, Z. Anorg. Allg. Chem. 228 (1936) 268–274.
[41] V. Tomashik, H.-L. Lukas, Materials Science International Team, Iron Systems, Part 4, 2008, pp. 284–318. http://dx.doi.org/10.1007/978-3-540-78644-3_20.
[42] N. Sano, M. Iwata, H. Hosoda, Y. Matsushita, Tetsu to Hagane 57 (1971) 1984–1989.
[43] M. Hillert, J. Alloys Compd. 320 (2001) 161–176.
[44] G. Mann, L. Van Vlack, Metall. Trans. B 7 (1976) 469–475.
[45] Y. Ito, N. Yonezawa, K. Matsubara, Tetsu to Hagane 65 (1979) 391–398.
[46] B.J. Skinner, F.D. Luce, Am. Mineral. 56 (1971) 1269–1296.
[47] M. Fischer, K. Schwerdtfeger, Metall. Trans. B 9 (1978) 635–641.
[48] J.S. Kirkaldy, H. Nakao, I.S.R. Clark, P.N. Smith, Can. Metall. Q. 12 (1973) 45–51.
[49] E. Schuermann, H.J. Stroesser, Arch. Eisenhuettenwes. 46 (1975) 761–766.
[50] R. Kiessling, C. Westman, J. Iron Steel Inst. 204 (1966) 377–379.
[51] R. Vogel, H. Baur, Arch. Eisenhuettenwes. 6 (1933) 495–500.
[52] C.W. Sherman, J. Chipman, J. Met. 4 (1952) 597–602.
[53] S. Ban-Ya, J. Chipman, Trans. Metall. Soc. AIME 245 (1969) 133–143.
[54] B.P. Burylev, L.S. Tsemekham, L.P. Mojsov, Izv. Russ. Akad. Nauk Met. 4 (2002) 17–19.
[55] E.T. Turkdogan, S. Ignatowicz, J. Pearson, J. Iron Steel Inst. 180 (1955) 349–354.
[56] M. Fischer, K. Schwerdtfeger, Metall. Trans. B 9 (1978) 631–634.
[57] M. Fischer, K. Schwerdtfeger, Metall. Trans. B 8 (1977) 467–470.
[58] C.W. Bale, P. Chartrand, S.A. Decterov, G. Eriksson, K. Hack, R. Ben Mahfoud, J. Melançon, A.D. Pelton, S. Petersen, CALPHAD 26 (2002) 189–228.
[59] C.W. Bale, E. Bélisle, P. Chartrand, S.A. Decterov, G. Eriksson, K. Hack, I.-H. Jung, Y.-B. Kang, J. Melançon, A.D. Pelton, C. Robelin, S. Petersen, CALPHAD 33 (2009) 295–311.
[60] A.T. Dinsdale, CALPHAD 15 (1991) 317–425.
[61] C.W. Bale, J.M. Toguri, Can. Metall. Q. 15 (1976) 305–318.
[62] R.C. Sharma, Y.A. Chang, Metall. Trans. B 10 (1979) 103–108.
[63] Y.Y. Chuang, K.C. Hsieh, Y.A. Chang, Metall. Trans. B 16 (1985) 277–285.
[64] R.C. Sharma, Y.A. Chang, Metall. Trans. B 11 (1980) 139–146.
[65] A.D. Pelton, Y.-B. Kang, Int. J. Mater. Res. 98 (2007) 907–917.
[66] Y.-B. Kang, A.D. Pelton, Modeling short-range ordering in liquids: The Mg–Al–Sn system, CALPHAD 34 (2010) 180–188.
[67] M. Hillert, L. Staffansson, Metall. Trans. B 6 (1975) 37–41.
[68] A. Guillermet, M. Hillert, B. Jansson, B. Sundman, Metall. Trans. B 12 (1981) 745–754.
[69] F. Kongoli, A. Pelton, Metall. Mater. Trans. B 30 (1999) 443–450.
[70] A. Pelton, M. Blander, Metall. Trans. B 17 (1986) 805–815.
[71] Y.-B. Kang, A.D. Pelton, P. Chartrand, C.D. Fuerst, CALPHAD 32 (2008) 413–422.
[72] Y.-B. Kang, I.-H. Jung, H.-G. Lee, CALPHAD 30 (2006) 235–247.
[73] Y.-B. Kang, I.-H. Jung, H.-G. Lee, CALPHAD 30 (2006) 226–234.
[74] E. Jak, P. Hayes, A.D. Pelton, S.A. Decterov, Int. J. Mater. Res. 9 (2007) 847–854.
[75] I.-H. Jung, S.A. Decterov, A.D. Pelton, Int. J. Mater. Res. 9 (2007) 816–825.
[76] C. Robelin, P. Chartrand, A.D. Pelton, J. Chem. Thermodyn. 36 (2004) 683–699.
[77] D. Lindberg, R. Backman, M. Hupa, P. Chartrand, J. Chem. Thermodyn. 38 (2006) 900–915.
[78] Y.-B. Kang, A.D. Pelton, Metall. Mater. Trans. B 40 (2009) 979–994.
[79] G. Effenberg, A. Prince, Materials Science International Team MSIT®, Light Metal Systems, Part 2, 2005, pp. 1–32. http://dx.doi.org/10.1007/10915967_4.
[80] V. Witusiewicz, F. Sommer, E. Mittemeijer, J. Phase Equilib. Diffus. 25 (2004) 346–354.
[81] M. Hillert, M. Jarl, CALPHAD 2 (1978) 227–238.
[82] H. Okamoto, T.B. Massalski, J. Phase Equilib. 12 (1991) 148–168.
[83] Steelmaking Data Sourcebook, Gordon and Breach Science Pub., Montreux, Swizerland, 1988.
[84] C.H.P. Lupis, Chemical Thermodynamics of Materials, Elsevier Science Publishing Co., Inc., NewYork, NY, 1983.